

A GREEN APPROACH FOR DYE DECONTAMINATION: ACTIVATED CARBON FROM HEMP WASTE

HARUN KAYA

*Malatya Turgut Özal University, Faculty of Engineering and Natural Sciences,
Department of Basic Sciences, 44000, Yeşilyurt, Malatya, Turkey*

✉ Corresponding author: harun.kaya@ozal.edu.tr

Received November 19, 2024

In this research, activated carbon was derived from hemp waste using a chemical activation technique, and methylene blue adsorption was tested. Hemp wastes were first carbonized at 500 °C, mixed at a 1:3 biochar/KOH ratio by mass, and activated at 800 °C. The equilibrium data's suitability to the Langmuir, Freundlich, and Harkin-Jura isotherms was investigated, and it was identified as compatible with the Langmuir isotherm. The maximum adsorption capacity (q_m) was determined as 400.25 mg/g. Adsorption kinetics were analyzed with intraparticle diffusion, pseudo-first and pseudo-second models, and determined to fit the pseudo-second-order kinetic model ($R^2 = 0.9934$). Since this method is inexpensive, it can be used effectively for eliminating methylene blue. From the results of the study, it is concluded that activated carbon from hemp waste is of strategic importance for environmental sustainability and water quality management.

Keywords: activated carbon, adsorption, hemp, dye, sustainability, water treatment

INTRODUCTION

Synthetic chemical compounds known as dyes can attach chemically to materials like paper, textiles, and fur to provide vivid colors. These compounds are frequently utilized in industrial processes to produce everyday items. It is known that more than 100,000 types of dyes are used in the dyeing and printing industry, and most of the resulting industrial wastewater is released into rivers and oceans. The dye residues found in wastewater are complex and unstable compounds, and these dissolved dye molecules are discharged into living ecosystems through wastewater. In environmentally sensitive systems, it is vital to treat this wastewater before discharge.¹

The most common methods for treating dye-containing wastewater include adsorption, flocculation, photocatalytic degradation, ion exchange, membrane filtration, electrochemical degradation, and advanced oxidation processes.²⁻⁴ Among them, adsorption has been recognized as one of the most effective water purification methods.⁵

The adsorption technique has been broadly applied in water treatment in recent years due to its high efficiency and ability to remove a wide range

of chemical pollutants, and it is a method with potential for industrial application.⁶ The most efficient material for adsorption purposes is activated carbon (AC). AC is an ideal material for adsorption, with good pore size, surface functional groups with high reactivity and high surface area. ACs are highly effective adsorbents, commonly utilized in media that can be either gaseous or aqueous, and consist of both organic and inorganic compounds.⁷ As the cost of commercially available ACs is high, it is essential to produce more cost-effective, sustainable and reusable ACs.⁸ In this context, activated carbons were produced from various agricultural wastes, such as mango peels and seeds,⁹ sugarcane,¹⁰ rosemary root,¹¹ corncob,¹² papaya bark fiber,¹³ cinnamon bark,¹⁴ chickpea stem,¹⁵ hemp fiber¹⁶ etc.

Methylene blue (MB) is an important aromatic compound with the chemical composition $C_{16}H_{18}ClN_3S$. Due to this aromatic ring, it is a highly toxic and carcinogenic dye. Since the degradation process of MB is complicated, it should be removed from wastewater before discharge.¹⁷

Hemp is a fast-growing plant that reaches maturity in 3–4 months. It can, therefore, capture carbon from the atmosphere more efficiently than many other plants and has a high biomass yield.¹⁸ Industrial hemp is a significant lignocellulosic biomass source whose production is on the rise. While hemp was previously cultivated for its fibers, today, its seeds are also cultivated for obtaining metabolites, such as terpenes and flavonoids, from the leaves and stems of the inflorescences.¹⁹ Hemp waste is increasing due to the increasing use of hemp in various industries, hemp regulations in some countries, and the growing demand for sustainable, environmentally friendly products.¹⁸

Since hemp cultivation has been banned in many countries for decades, academic studies on the use of this plant and its wastes in various fields are still of great interest. These wastes are biomass sources that can be suitable for activated carbon production. Therefore, in this study, activated carbon produced from the hemp plant's root and stem parts was used as adsorbent. The adsorption mechanism of MB, which is widely used to color cotton, wool and silk, was investigated. The study results showed that hemp wastes were highly successful in MB adsorption.

EXPERIMENTAL

Preparation of AC

This study utilized waste parts of hemp plants grown at the Malatya Turgut Özal University, Faculty of Agriculture. Hemp wastes underwent a cleaning process using distilled water to eliminate soil and other contaminants, followed by drying at 80 °C for 48 hours. The cleaned raw samples were carbonized at 500 °C for 1 hour, at a heating rate of 10 °C/min at a flow rate of 150 mL/min N₂ gas. Carbonization was carried out in a steel reactor using a Protherm PZF 12/50/700 model three-zone tubular furnace. The carbonized product was prepared for activation by impregnating KOH at a ratio of 1:3. The chemical activation of impregnated carbonized hemp was performed at 800 °C for 1 hour, with a heating rate of 10 °C/min under a flow of 150 mL/min N₂ gas. Elemental analysis (LECO CHNS-932), Scanning Electron Microscopy (Leo EV040) and Brunauer, Emmet and Teller (Micromeritics Gemini VII) analysis were performed to determine the morphology of activated carbon.

Adsorption studies

Batch adsorption was carried out for 1–300 min at different concentrations of MB (50, 100, 200 and 400

ppm) using 0.02 g activated carbon. The concentration of MB in the solution was determined at a wavelength of 665 nm using a UV-vis spectrophotometer (Cary 60, Agilent Technologies). The removal rate and the adsorption capacity (q_e) were calculated by Equations (1) and (2), respectively:¹¹

$$\text{Removal (\%)} = \frac{(C_o - C_e)}{C_o} \times 100 \quad (1)$$

$$q_e = \frac{(C_o - C_e)}{m} \times V \quad (2)$$

where: C_o – initial concentration (mg/L), C_e – final concentration (mg/L), m – the mass of the adsorbent (g), V – the volume of the solution (L).

The Langmuir, Freundlich and Harkin-Jura isotherms were used to elucidate the adsorption mechanism by Equations (3–5):²⁰

$$\text{Langmuir: } \frac{C_e}{q_e} = \frac{1}{k_L q_m} + \frac{C_e}{q_m} \quad (3)$$

$$\text{Freundlich: } \log(q_e) = \log(k_F) + \frac{1}{n} \log(C_e) \quad (4)$$

$$\text{Harkin-Jura: } \frac{1}{q_e^2} = \left[\frac{B_{HJ}}{A_{HJ}} \right] - \left[\frac{1}{A_{HJ}} \right] \log(C_e) \quad (5)$$

where: C_e – the equilibrium concentration (mg/L), q_e – adsorption capacity (mg/g), q_m – maximum adsorption capacity (mg/g), k_L – Langmuir constant (L/mg), k_F – multilayer adsorption capacity (mg/g), n – intensity parameter, B_{HJ} and A_{HJ} – Harkins-Jura constants.

Adsorption kinetics was examined by the pseudo-first, pseudo-second and intraparticle diffusion models (Eqs. 6–8):^{11,21–23}

$$\text{Pseudo-First: } \log(q_e - q_t) = \log(q_e) - \left(\frac{k_1}{2.303} \right) t \quad (6)$$

$$\text{Pseudo-Second: } \frac{t}{q_t} = \frac{1}{k_2 q_e^2} + \frac{t}{q_e} \quad (7)$$

$$\text{Intraparticle Diffusion: } q_t = k_i t^{0.5+c} \quad (8)$$

where: q_t – the amount of adsorbate uptake on a per-unit-mass basis of the adsorbent at time t (mg/g), q_e – the amount of adsorbate uptake on a per-unit-mass basis of the adsorbent at equilibrium (mg/g), k_1 , k_2 , k_i , and c denote the corresponding rate constants, while t (min) represents the contact time.

RESULTS AND DISCUSSION

Characterization of activated carbons

Elemental analysis results of raw hemp and 1:3 KOH impregnated activated carbon (AC) are given in Table 1. As depicted in Table 1, the C content, which was about 70% in raw hemp, and increased to 74% in activated carbon prepared by impregnating KOH at a ratio of 1:3, while the H content decreased from 2.32% to 0.28%. No significant change was observed in N and S contents.

The BET results of raw hemp and AC are given in Table 2. The hysteresis in Figure 1 showed that the pore type in activated carbon is consistent with Type IV-H2 (inkbottle-shaped pore).²⁴

Table 1
Elemental analysis results of raw hemp and AC

Sample	C%	H%	N%	S%	*O%
Raw hemp	70.11	2.32	0.31	0.03	27.23
AC	74.24	0.28	0.35	0.02	25.11

*by difference

Table 2
BET analysis results of raw hemp and AC

Sample	BET surface area (m ² /g)	Micropore area (m ² /g)	Mesopore area (m ² /g)	Average pore diameter d _p (4 V/A by BET) (nm)
Raw hemp	167.36	151.74	15.62	1.7763
AC	1826.86	536.42	1290.44	2.323

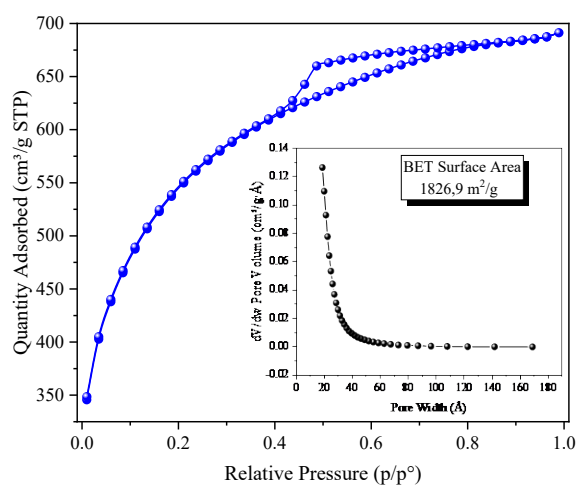


Figure 1: N₂ adsorption isotherms

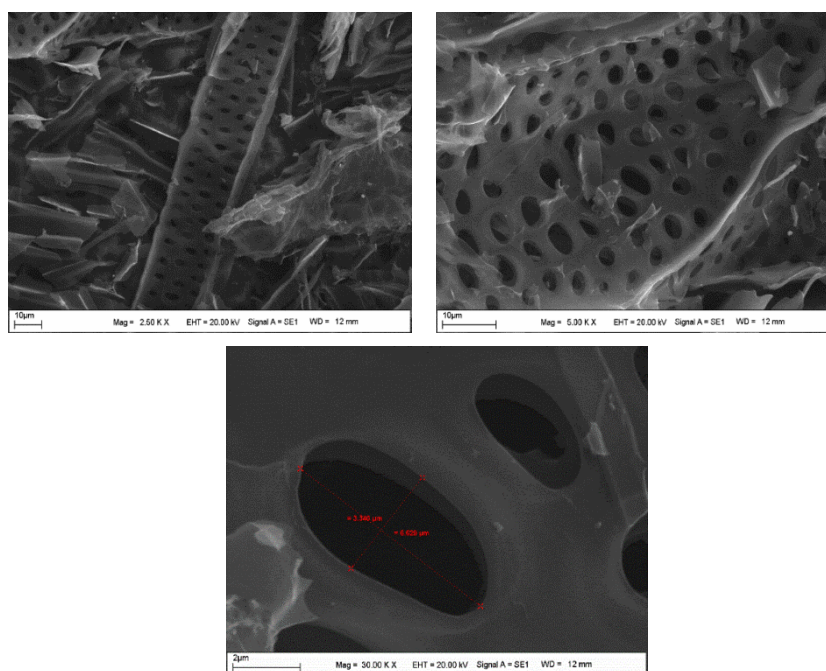


Figure 2: SEM images of AC

From Table 2, it is seen that raw hemp has a unique porosity. This is because there are channels in the stem of such plants that carry nutrients from the stem to the leaves, flowers and seeds.

Due to these channels, it is natural for plants like hemp to have such pores.²⁵ The BET surface area of raw hemp was 167.36 m²/g and the surface area after activation was 1826.86 m²/g. Given that commercial activated carbons typically exhibit a surface area exceeding 1000 m²/g, it is evident that the activated carbon synthesized through chemical activation in this study demonstrates a notably high surface area. It is documented in the literature that the surface areas of activated carbons derived from hemp typically fall within the range of 1100-3241 m²/g.²⁶⁻²⁹ Moreover, mesopores and micropores in activated carbon improve the adsorption of larger molecules.³⁰

The more mesopores with an average pore diameter of 2-10 nm, the greater the adsorption capacity of the activated carbon. Taking into account the micro- and mesopore areas presented in Table 2, it can be inferred that the obtained activated carbon will possess a high adsorption capacity.

Figure 2 shows SEM images of activated carbon obtained from hemp. The images show the presence of porous channels, with pore diameters varying between 1 and 5 µm. The images support the ink-bottle-shaped pore structure that causes the hysteresis seen in Figure 1.

Adsorption isotherms

Adsorption isotherms help describe the adsorbent's equilibrium performance at constant temperature. These isotherms are established by contact of the adsorbent with the adsorbate for a sufficient period of time. This period refers to the time when the interfacial concentration dynamically reaches equilibrium with the current concentration of adsorbate in the solution. Understanding the adsorption equilibrium is crucial for comprehending the adsorption process accurately. The importance of adsorption isotherms of porous materials, CO₂ capture, gas storage, catalysis, chemical separation, *etc.*, contains important balance information that is needed in many areas. Predicting the overall adsorption behavior can be achieved by modeling the isotherm data using linear analysis as an alternative mathematical approach.²⁰

Major equations (Langmuir, Freundlich, Temkin, Harkin-Jura, Dubinin-Radushkevich, Koble-Corrigan, *etc.*) are commonly employed for

describing the adsorption isotherm. These equations help describe the adsorbent's surface properties and the relationship between the adsorbate and the adsorbent. The empirical equations for the adsorption isotherms used in this research are given in Equations (3-4).

The Langmuir adsorption isotherm is founded on the kinetic principle that the adsorption process on a solid surface entails the desorption or evaporation of molecules, with a zero deposition rate attributed to the constant bombardment of molecules onto the surface. This model assumes all sites have equal attraction to the adsorbate and no adsorbate migration in the surface plane. The partition factor R_L is a dimensionless term in the Langmuir isotherm (Eq. 9):

$$R_L = \frac{1}{1 + k_L C_0} \quad (9)$$

The amount of saturated monolayer adsorption per unit weight of adsorbent (q_m) is calculated as in Equation (10):

$$q_e = \frac{q_m k_L C_e}{1 + k_L C_e} \quad (10)$$

If $R_L > 1$, adsorption is unfavorable; if $R_L = 1$, the isotherm is linear (first order); if $0 < R_L < 1$, adsorption is spontaneous and if $R_L = 0$, adsorption is irreversible.³¹ The graphs of Langmuir are given in Figure 3. As the calculated R_L value is 0.6135, it is possible to assert that adsorption takes place spontaneously. The Langmuir constant was calculated as k_L : 1.25×10^{-2} and maximum adsorption capacity q_m : 400.25 mg/g. Xue *et al.* examined the adsorption of methylene blue (MB) after activating *Ashitaba* seeds with $ZnCl_2$. According to the Langmuir isotherm model, they calculated a maximum adsorption capacity (q_m) of 323.54 mg/g.³²

Freundlich adsorption isotherm describes a reversible adsorption process. Unlike Langmuir, this model is not constrained to monolayer formation, but can be extended to encompass multilayer adsorption. 'n' represents the intensity of adsorption or surface heterogeneity, reflecting the diversity of adsorbate sites. The more heterogeneous the surface, the closer n is to 0. If n is between 0 and 1 ($0 < n < 1$), adsorption is favorable; if it is greater than 1, adsorption is unfavorable; if it is equal to 1, adsorption is irreversible.³³

Figure 4 shows the Freundlich graphs. n is determined from the slope of the graph plotted against $\log C_e$ versus $\log q_e$ values. Since the n value is 0.9615, it is possible to state that adsorption takes place on homogeneous surfaces.

The multilayer adsorption capacity (k_F) was 5.11 mg/g. This value, which is quite low compared to the Langmuir one, confirms that adsorption occurs in a single layer.

The Harkin-Jura isotherm model elucidates multilayer adsorption and the uneven distribution of pores across the adsorbent surface.³⁴ Since the Harkins-Jura isotherm model, like the Freundlich model, is applied to multilayer adsorption on heterogeneous surfaces, it supports the Freundlich

isotherm model in this respect.³⁵ This isotherm's constants are obtained from the slope ($1/A_{HJ}$) and intercept (B_{HJ}/A_{HJ}) of the graph plotted against $\log C_e$ versus $1/q_e^2$.³⁶ The graphs of Harkin-Jura are given in Figure 5. Harkin-Jura constants were calculated as A_{HJ} : 2×10^4 and B_{HJ} : 2. Since the correlation coefficient (R^2) is low (0.70), it is possible to assert that adsorption occurs in a single layer rather than in multiple layers.

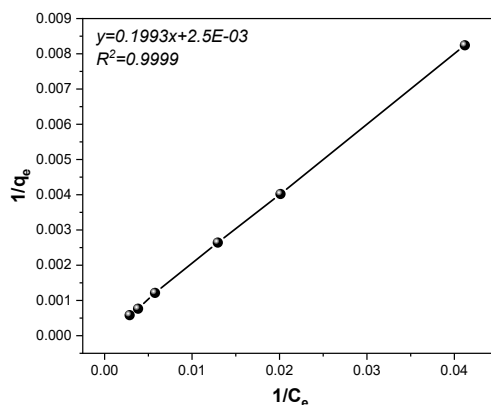


Figure 3: Graph of Langmuir adsorption isotherm

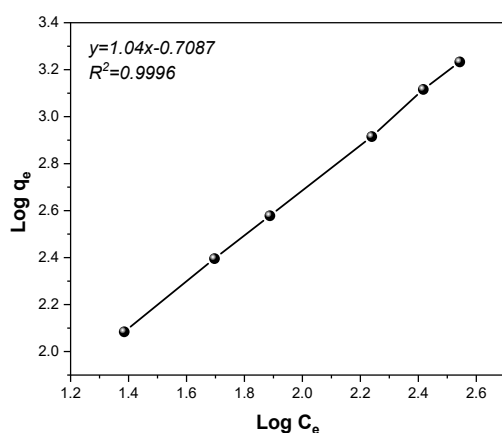


Figure 4: Graph of Freundlich adsorption isotherm

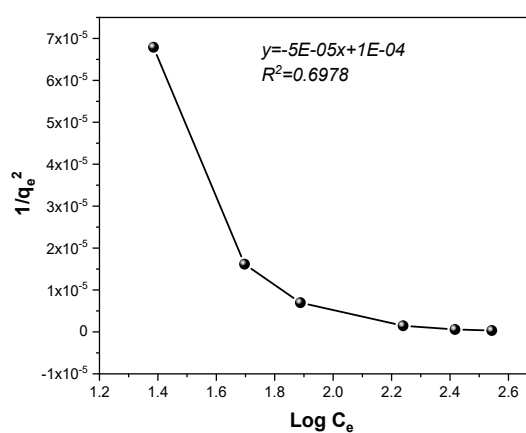


Figure 5: Graph of Harkin-Jura adsorption isotherm

Table 3
Maximum adsorption capacities of various activated carbons towards MB

Adsorbent	qm (mg/g)	Ref.
Walnut shell	315	39
Nut shell	87	40
Peanut shell	110	41
Sugarcane bagasse waste	137	42
Bamboo waste	285	43
Lavandin (<i>Lavandula</i> genus) biomass	306	44
Raspberry (<i>Rubus idaeus</i>) leaves	245	45
Hemp hurd powder	240	46
Hemp waste	400	Present study

Among the adsorption isotherm models, the Langmuir model is found to be the most suitable. Uddin *et al.* also reported the applicability of the Langmuir model in the adsorption of MB using activated carbon derived from peanut shells via KOH activation.³⁷ Similarly, Hayeeye *et al.* utilized activated carbons obtained from the agricultural waste – *Dialium cochinchinense* seeds, activated with H_3PO_4 , KOH, and $ZnCl_2$, for the removal of Reactive Red 120 (RR120) dye, and

they observed a good fit to the Langmuir model for the adsorption process.³⁸

The maximum adsorption capacities of AC towards MB, as compared to previous literature data, are presented in Table 3. The q_m values obtained in this study are found to be higher than those reported for other activated carbons in the literature.

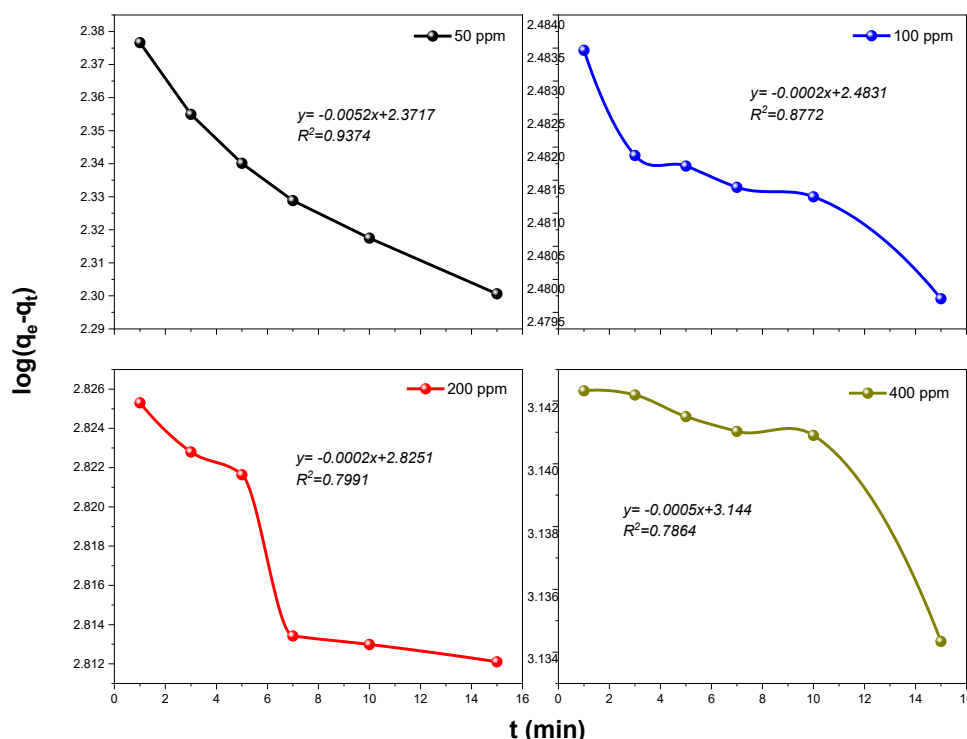


Figure 6: Graphs of pseudo-first kinetic model at different concentrations

Adsorption kinetics

Adsorption constitutes a complex process involving a combination of surface adsorption and diffusion into pores. Estimating the completion time of adsorption is one of the crucial parameters in the adsorption process. The transfer of ions to the adsorbent surface, the filling of surface pores, the diffusion of particles, and other related factors play crucial roles in determining the adsorption time between the adsorbent and the adsorbate. Hence, determining the adsorption rate will require investigating the compatibility of experimental results with various kinetic models. The pseudo-first, pseudo-second, and intraparticle diffusion kinetic models were used for this purpose.²²

The pseudo-first order, or Lagergren's, is the most widely used kinetic model for a liquid-solid adsorption system.⁴⁷ The model describes the adsorption kinetics by the ordinary first-order differential equation (Eq. 6). The pseudo-first-order kinetic graphs drawn as a function of the contact time (t) of $\ln(q_e - q_t)$ for each concentration are given in Figure 6. As depicted in Figure 6, the highest R^2 value (0.9374) was achieved at a dye concentration of 50 ppm. At this concentration, the constant was calculated as $k_1: 12 \times 10^{-3}$, and the amounts of adsorbate uptake per unit mass of the adsorbent at equilibrium q_e were 235.34 mg/g.

The pseudo-second order model, also known as the Blanchard model, is expressed by a quadratic differential equation (Eq. 7), since it is based on the

fact that adsorption occurs at two surface regions.⁴⁸ The pseudo-second order kinetic graphs drawn as a function of the contact time (t) of t/q_t for each concentration are given in Figure 7. From Figure 7, the highest R^2 value (0.9934) was also obtained at 50 ppm dye concentration. At this concentration, the constant was calculated as k_2 : 2.58×10^{-3} and the amounts of adsorbate uptake per unit mass of the adsorbent at equilibrium q_e : 66.23 mg/g.

When comparing the pseudo-first and pseudo-second kinetic data, the adsorption exhibited better agreement with the pseudo-second model, as indicated by higher R^2 and q_e values. Zhou *et al.* indicated that the most suitable model for MB adsorption from *Eucommia ulmoides* biomass,

activated with H_3PO_4 , is the pseudo-second-order model.⁴⁹

In a solid-liquid sorption process, the transfer of adsorbate is typically characterized by film diffusion, intraparticle diffusion, or a combination of both. The mechanism underlying the adsorption process is the most commonly used technique to identify the adsorbed amount against time, which is an internal diffusion graph. The graph of $t^{0.5}$ versus q_t at different initial solution concentrations gives the k_i value. It can offer multiple linearities that refer to two or more steps in the adsorption process. Intraparticle diffusion coefficient, k_i , is obtained by Equation (8).

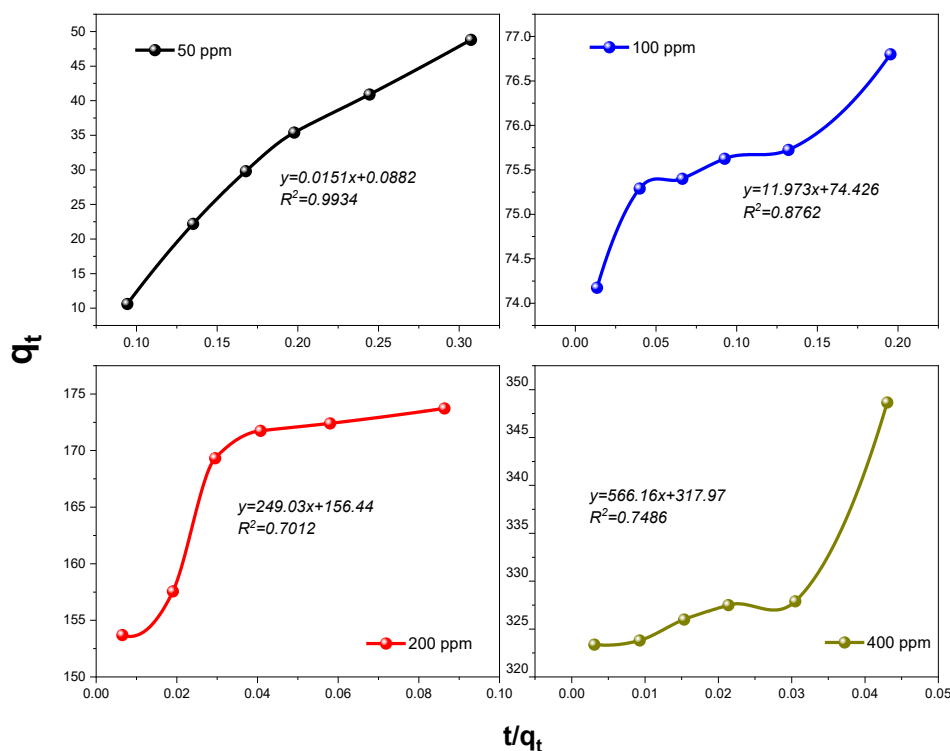


Figure 7: Graphs of pseudo-second kinetic model at different concentrations

Table 4
Kinetic parameters and regression coefficients obtained from kinetic models

C_i (ppm)	Pseudo-first order			Pseudo-second order			Intraparticle diffusion		
	k_1 (10^{-3})	q_e	R^2	k_2 (10^{-3})	q_e (10^{-3})	R^2	k_i	c	R^2
50	12	235.34	0.9374	2.58	66230	0.9934	3.3155	37.226	0.9911
100	0.461	304.16	0.8772	1904	84	0.8762	0.7887	73.557	0.9131
200	0.461	668.50	0.7991	396340	4.016	0.7012	7.6212	147.8	0.8296
400	1.15	1393.16	0.7864	1008400	1.766	0.7486	6.9823	314.11	0.8023

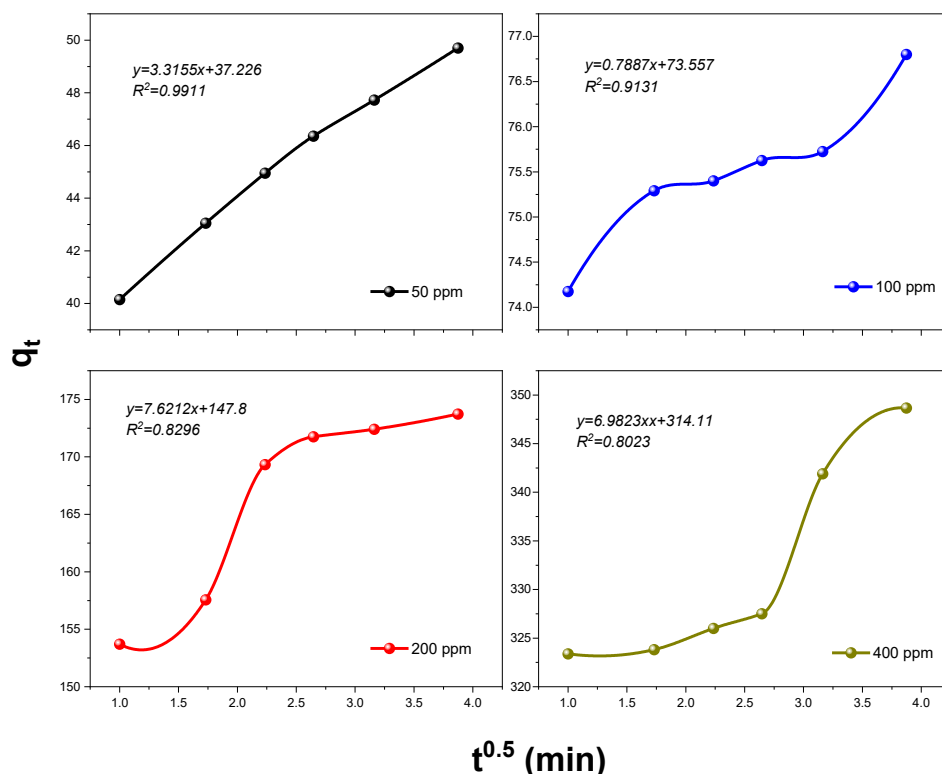


Figure 8: Graphs of intraparticle kinetic model at different concentrations

The initial sharp increase represents the external surface adsorption or instantaneous adsorption stage. The second part is the gradual adsorption stage, in which the intraparticle diffusion rate is controlled. The third is the final equilibrium stage, in which the intraparticle diffusion begins to slow down due to the deficient solute concentration in the solution. The intraparticle diffusion rate is determined from the slope of the slightly inclined part.⁵⁰ The intraparticle kinetic graphs drawn as a function of the square root contact time ($t^{0.5}$) of q_t for each concentration are given in Figure 8.

The intraparticle diffusion constant (k_i) was calculated as 3.32. This suggests that the outer adsorption layer of activated carbon is thick.⁵¹ It was also observed that R^2 values decreased with increasing concentration. Kinetic parameters and regression coefficients are given in Table 4. When Table 4 is examined, the R^2 values in each kinetic model decrease with increasing concentration. Therefore, it was concluded that the optimal concentration for adsorption is 50 ppm.

CONCLUSION

In this research, AC was obtained from hemp wastes by a two-stage chemical activation

technique and its adsorption efficiency at different dye concentrations was studied in the context of MB elimination from wastewater. The Langmuir model was the most compatible when the adsorption data were analyzed with isotherm models ($R^2 = 0.9999$). According to the Langmuir isotherm, the maximum adsorption capacity was calculated as 400.25 mg/g, which is a very high value. Thus, it can be stated that adsorption occurs in a monolayer on homogeneous surfaces. When the adsorption equilibrium data underwent analysis with kinetic models, the pseudo-second kinetic model demonstrated the highest compatibility, with an R^2 value of 0.9934. The fit to all three kinetic models decreased as the dye concentration increased. According to the results, the AC obtained from hemp wastes has proved to be very effective in removing MB.

REFERENCES

- ¹ İ. Gözetin and A. Savran, *J. Nat. Appl. Sci. East.*, **4**, 48 (2021)
- ² A. H. Jawad, A. S. Abdulhameed, L. D. Wilson, S. S. A. Syed-Hassan, Z. A. Alothman *et al.*, *Chin. J. Chem. Eng.*, **32**, 281 (2021), <https://doi.org/10.1016/j.cjche.2020.09.070>
- ³ J. Joseph, R. C. Radhakrishnan, J. K. Johnson, S. P. Joy and J. Thomas, *Mater. Chem. Phys.*, **242**, 122488

- (2020), <https://doi.org/10.1016/j.matchemphys.2019.122488>
- ⁴ Y. Kuang, X. Zhang and S. Zhou, *Water*, **12**, 587 (2020), <https://doi.org/10.3390/w12020587>
- ⁵ A. Fekaoui, E. A. Varol, G. Henini, U. T. Un and Y. Laidani, *Cellulose Chem. Technol.*, **58**, 379 (2024), <https://doi.org/10.35812/CelluloseChemTechnol.2024.58.37>
- ⁶ M. Gören, H. B. Murathan, N. Kaya and A. M. Murathan, *J. Polytech.*, **26**, 283 (2023), <https://doi.org/10.2339/politeknik.989900>
- ⁷ H. Debbache, A. A. Amor, F. Z. Ayachi-Amor, R. Khiari, Y. Moussaoui *et al.*, *Cellulose Chem. Technol.*, **58**, 1149 (2024), <https://doi.org/10.35812/CelluloseChemTechnol.2024.58.98>
- ⁸ T. H. Do, N.Q. Dung, M. N. Chu, D. Van Kiet, T. T. K. Ngan *et al.*, *Mater. Today Proc.*, **38**, 3405 (2021), <https://doi.org/10.1016/j.matpr.2020.10.834>
- ⁹ N. S. Razali, A. S. Abdulhameed, A. H. Jawad, Z. A. Alothman, T. A. Yousef *et al.*, *Molecules*, **27**, 6947 (2022), <https://doi.org/10.3390/molecules27206947>
- ¹⁰ F. Mohamed, M. Shaban, S. K. Zaki, M. S. Abd-Elсамie, R. Sayed *et al.*, *Sci. Rep.*, **12**, 18031 (2022), <https://doi.org/10.1038/s41598-022-22421-8>
- ¹¹ T. Bouzid, A. Grich, A. Naboulsi, A. Regti, A. A. Tahiri *et al.*, *Inorg. Chem. Commun.*, **158**, 111544 (2023), <https://doi.org/10.1016/j.inoche.2023.111544>
- ¹² T. H. Tran, A. H. Le, T. H. Pham, X. C. Nguyen, A. K. Nadda *et al.*, *Environ. Res.*, **212**, 113178 (2022), <https://doi.org/10.1016/j.envres.2022.113178>
- ¹³ S. T. Nipa, N. R. Shefa, S. Parvin, M. A. Khatun, M. J. Alam *et al.*, *Results Eng.*, **17**, 100857 (2023), <https://doi.org/10.1016/j.rineng.2022.100857>
- ¹⁴ B. Yardımcı and N. Kanmaz, *J. Environ. Chem. Eng.*, **11**, 110254 (2023), <https://doi.org/10.1016/j.jece.2023.110254>
- ¹⁵ N. Genli, S. Kutluay, O. Baytar and Ö. Şahin, *Int. J. Phytorem.*, **24**, 88 (2022), <https://doi.org/10.1080/15226514.2021.1926911>
- ¹⁶ G. Viscusi, E. Lamberti and G. Gorrasi, *Chemosphere*, **288**, 132614 (2022), <https://doi.org/10.1016/j.chemosphere.2021.132614>
- ¹⁷ E. Misran, O. Bani, E. M. Situmeang and A. S. Purba, *Alexandria Eng. J.*, **61**, 1946 (2022), <https://doi.org/10.1016/j.aej.2021.07.022>
- ¹⁸ N. Muttil, S. Sadath, D. Coughlan, P. Paresi and S. K. Singh, *Int. J. Integr. Eng.*, **16**, 1 (2024), <https://doi.org/10.30880/ijie.2024.16.02.001>
- ¹⁹ M. Staf, V. Šrámek and M. Pohořelý, *Energies*, **16**, 1202 (2023), <https://doi.org/10.3390/en16031202>
- ²⁰ M. A. Al-Ghouti and D. A. Da'ana, *J. Hazard. Mater.*, **393**, 122383 (2020), <https://doi.org/10.1016/j.jhazmat.2020.122383>
- ²¹ Q. Hu, S. Pang and D. Wang, *Sep. Purif. Rev.*, **51**, 281 (2022), <https://doi.org/10.1080/15422119.2021.1922444>
- ²² Z. M. Şenol, S. Şimşek, A. Özer and D. Şenol Arslan, *J. Radioanal. Nucl. Chem.*, **327**, 159 (2021), <https://doi.org/10.1007/s10967-020-07481-2>
- ²³ S. Zafar, N. Khalid, M. Daud and M. L. Mirza, *The Nucleus*, **52**, 14 (2015), <https://doi.org/10.71330/thenucleus.2015.659>
- ²⁴ K. S. W. Sing, D. H. Everett, R. A. W. Haul, L. Moscou, R. A. Pierotti *et al.*, *Pure Appl. Chem.*, **57**, 603 (1985), <http://dx.doi.org/10.1351/pac198557040603>
- ²⁵ A. A. Korkmaz and Y. Önal, *Konya J. Eng. Sci. (KONJES)*, **10**, 29 (2022), <https://doi.org/10.36306/konjes.967894>
- ²⁶ M. Z. Hossain, W. Wu, W. Z. Xu, M. B. Chowdhury, A. K. Jhavar *et al.*, *J. Carbon Res.*, **4**, 38 (2018), <https://doi.org/10.3390/c4030038>
- ²⁷ S. Liu, L. Ge, S. Gao, L. Zhuang, Z. Zhu *et al.*, *Compos. Commun.*, **5**, 27 (2017), <https://doi.org/10.1016/j.coco.2017.06.002>
- ²⁸ J. Zhang, J. Gao, Y. Chen, X. Hao and X. Jin, *Results Phys.*, **7**, 1628 (2017), <https://doi.org/10.1016/j.rinp.2017.04.028>
- ²⁹ R. Yang, G. Liu, M. Li, J. Zhang and X. Hao, *Micropor. Mesopor. Mater.*, **158**, 108 (2012), <https://doi.org/10.1016/j.micromeso.2012.03.004>
- ³⁰ T. C. Chandra, M. M. Mirna, Y. Sudaryanto and S. Ismadji, *Chem. Eng. J.*, **127**, 121 (2007), <https://doi.org/10.1016/j.cej.2006.09.011>
- ³¹ Y. Toptaş, B. Yavuz, A. Aksoğan Korkmaz and Y. Önal, *Int. J. Environ. Anal. Chem.*, **1** (2024), <https://doi.org/10.1080/03067319.2024.2346192>
- ³² H. Xue, X. Wang, Q. Xu, F. Dhaouadi, L. Sellaoui *et al.*, *Chem. Eng. J.*, **430**, 132801 (2022), <https://doi.org/10.1016/j.cej.2021.132801>
- ³³ N. Ayawei, A. N. Ebelegi and D. Wankasi, *J. Chem.*, **2017**, 1 (2017), <https://doi.org/10.1155/2017/3039817>
- ³⁴ I. Javed, M. A. Hanif, U. Rashid, F. Nadeem, F. A. Alharthi *et al.*, *Water*, **14**, 2600 (2022), <https://doi.org/10.3390/w14172600>
- ³⁵ E. N. Heybet, V. Ugraskan, B. Isik and O. Yazici, *Int. J. Biol. Macromol.*, **193**, 88 (2021), <https://doi.org/10.1016/j.ijbiomac.2021.10.084>
- ³⁶ İ. Küçük, *Cumhuriyet Sci. J.*, **42**, 843 (2021)
- ³⁷ M. T. Uddin, M. Rukanuzzaman and M. A. Islam, *Desalin. Water Treat.*, **280**, 60 (2022), <https://doi.org/10.5004/dwt.2022.28961>
- ³⁸ F. Hayeeye, A. Benhawan and M. Sattar, *Desalin. Water Treat.*, **269**, 200 (2022), <https://doi.org/10.5004/dwt.2022.28751>
- ³⁹ J. Yang and K. Qiu, *Chem. Eng. J.*, **165**, 209 (2010), <https://doi.org/10.1016/j.cej.2010.09.019>
- ⁴⁰ J. N. Nsami and J. K. Mbadcam, *J. Chem.*, **2013**, 469170 (2013), <https://doi.org/10.1155/2013/469170>
- ⁴¹ I. Sanou, H. Bamogo, A. Sanou, M. Ouedraogo, L. Saadi *et al.*, *Chem. Afr.*, **7**, 2777 (2024), <https://doi.org/10.1007/s42250-024-00927-0>
- ⁴² A. H. Jawad, A. S. Abdulhameed, N. N. Bahrudin, N. M. F. Hum, S. N. Surip *et al.*, *Water Sci. Technol.*, **84**, 1858 (2021), <https://doi.org/10.2166/wst.2021.355>

- ⁴³ A. Hapiz, A. H. Jawad, L. D. Wilson, A. S. Abdulhameed and Z. A. Alothman, *Biomass Convers. Biorefin.*, **14**, 31607 (2024), <https://doi.org/10.1007/s13399-023-04868-5>
- ⁴⁴ X. Li, E. Bonjour, P. Jame, P. Kuzhir and C. Hurel, *Biomass Convers. Biorefin.*, **14**, 19723 (2024), <https://doi.org/10.1007/s13399-023-04122-y>
- ⁴⁵ G. Mosoarca, S. Popa, C. Vancea, M. Dan and S. Boran, *Polymers*, **14**, 1966 (2022), <https://doi.org/10.3390/polym14101966>
- ⁴⁶ P. Xu, B. Li, J. Yu, L. Liu, J. Xu *et al.*, *Sci. Adv. Mater.*, **11**, 661 (2019), <https://doi.org/10.1166/sam.2019.3482>
- ⁴⁷ M. Benjelloun, Y. Miyah, G. A. Evrendilek, F. Zerrouq and S. Lairini, *Arabian J. Chem.*, **14**, 103031 (2021), <https://doi.org/10.1016/j.arabjc.2021.103031>
- ⁴⁸ H. Moussout, H. Ahlafi, M. Aazza and H. Maghat, *Karbala Int. J. Mod. Sci.*, **4**, 244 (2018), <https://doi.org/10.1016/j.kijoms.2018.04.001>
- ⁴⁹ Q. Zhou, L. Qiu and M. Zhu, *Ind. Crop. Prod.*, **187**, 115537 (2022), <https://doi.org/10.1016/j.indcrop.2022.115537>
- ⁵⁰ N. Kanmaz, *J. Inst. Sci. Technol.*, **12**, 1436 (2022), <https://doi.org/10.21597/jist.1079143>
- ⁵¹ J. P. Vareda, *J. Mol. Liq.*, **376**, 121416 (2023), <https://doi.org/10.1016/j.molliq.2023.121416>